Received: 12 March 2023 | Revised: 16 July 2023 | Accepted: 21 August 2023

DOI: 10.1002/eqe.4004

RESEARCH ARTICLE

WILEY

Influence of corrosion on failure modes and lifetime seismic vulnerability assessment of low-ductility RC frames

Shivang Shekhar[1] | **Fabio Freddi**[2] | **Jayadipta Ghosh**[3] | **Devang Lad**[2]

[1]School of Civil and Environmental Engineering, Indian Institute of Technology Mandi, Mandi, India

[2]Department of Civil, Environmental & Geomatic Engineering, University College London, London, UK

[3]Department of Civil Engineering, Indian Institute of Technology Bombay, Mumbai, India

Correspondence
Fabio Freddi Department of Civil, Environmental & Geomatic Engineering, University College London, London, UK.
Email: f.freddi@ucl.ac.uk

Funding information
Science and Engineering Research Board, Grant/Award Numbers: SRG/2021/001574, CRG/2021/000777

Abstract

Corrosion of reinforced concrete (RC) structures constitutes a critical form of environmental deterioration and may significantly increase the vulnerability of old non-seismically designed buildings during earthquake events. This study proposes a probabilistic framework to evaluate the influence of corrosion deterioration on the lifetime seismic fragility of low-ductility RC frame buildings. In contrast to limited past literature on this topic, the proposed framework offers novel contributions. This is one of the first study to consider potential alteration in failure modes of building components (from flexure to flexure-shear) due to the time-dependent aging process. Numerical models validated with past experimental test results are utilized to capture these failure modes, which are particularly relevant for low ductility RC frames designed prior to the introduction of modern seismic codes. Secondly, given the gamut of uncertainties associated with the corrosion process, this study develops condition-dependent seismic fragility functions independent from an assumed exposure scenario, as often done in literature. These functions can be easily adopted by design engineers and stakeholders for prompt fragility assessment, and subsequent decision-making without the need for computationally expensive finite element (FE) model runs. The proposed framework is demonstrated on a benchmark three-story RC frame that considers time-varying seismic demand models and damage state thresholds while accounting for the uncertain corrosion deterioration process and ground motion record-to-record variability.

KEYWORDS

aging and deterioration, low-ductility reinforced concrete frames, seismic fragility curves, time-dependent damage states thresholds

1 | INTRODUCTION

A predominant phenomenon that affects the structural performance of reinforced concrete (RC) buildings relates to durability aspects from exposure to harsh environmental stressors. When located in adverse environmental conditions (e.g., coastal areas and industrial sites), RC buildings are typically affected by aging and deterioration of their structural

components. Corrosion in RC structures is the most widely observed cause for chemical deterioration that substantially affects their service life.[1,2] This degradation mechanism typically leads to a significant reduction in the cross-sectional area of reinforcing steel along with alteration in mechanical properties of concrete and steel—leading to loss of load-carrying capacity of sections, elements, and sometimes the whole structure. Past studies revealed that 70%–90% of the deterioration in RC buildings is a consequence of corrosion of RC components.[3] Furthermore, corrosion deterioration is estimated to cost around 2.5 trillion USD (United States Dollars) globally, which is comparable to 3.4% of the global Gross Domestic Product (GDP).[4] For some countries, this can be as high as 5% of their annual GDP.[4] In addition to continuous exposure to environmental hazards, when located in moderate to high seismic regions, RC buildings are also exposed to intermittent seismic threats along their service life.

Across the globe, old and typically non-ductile RC buildings have experienced substantial damage and, in certain instances, collapse due to earthquake events, resulting in enormous economic and human losses. This has been highlighted by the very recent earthquake sequence that struck southern Turkey near the northern border with Syria. On February 6th 2023, a 7.8 M_w mainshock was followed 11 min later by a 6.7 M_w aftershock and, after a few hours, by a 7.5 M_w aftershock (https://earthquake.usgs.gov/) causing thousands of building collapses and a huge amount of casualties. Many other historical events highlighted the significant consequences of "rare" high-intensity earthquakes, such as the 1976 Tangshan earthquake, which resulted in 255,000 casualties and 10 billion USD loss, and the 2011 Tohoku earthquake, which resulted in 30,000 casualties and a 235 billion USD loss.[5,6] Such consequences are often related to the high vulnerability of existing constructions, with corrosion deterioration playing a significant role, in some situations.

While extensive research has been carried out on the influence of corrosion deterioration on the seismic performance of civil infrastructure systems (e.g., highway bridges),[7–9] there is a growing need for similar explorations for deteriorating RC buildings. Even though seismic damage to highway bridges disrupts access to critical lifeline facilities, RC buildings carry a higher risk of injuries and fatality to human lives. Moreover, building stock forms the vastest part of the built environment, and earthquake-induced damage to building structures could result in extensive business interruptions, inadequate functioning of strategic facilities, and disruption of manufacturing units. Recognizing these critical aspects, more research studies are focusing on the seismic performance assessment of deteriorating RC buildings.

Among the early literature on this topic, Pitilakis et al.[10] emphasized the adverse effects of corrosion deterioration on the time-dependent seismic performance of low-, mid-, and high-rise moment-resisting frames through probabilistic modeling of the degradation mechanism. Couto et al.[11] studied the influence of varying corrosion rates on the fragility assessment of aging RC building frames built between 1960 and 1980 in Portugal. For seismic fragility assessment, time-dependent corrosion deterioration effects such as rebar area reduction and concrete strength reduction were considered in the numerical model. Results revealed that the failure probability of corroded frames increases by as much as 20% due to corrosion, and concrete strength degradation had a pronounced influence on seismic capacity than rebar area reduction. Di Sarno and Pugliese[12] numerically investigated the seismic response of a RC building for different levels of exposure and degradation conditions. The primary and secondary effects of corrosion deterioration of RC members, such as reduction in rebar area and in the mechanical properties of steel and concrete, were considered. The non-linear dynamic analyses revealed that corrosion deterioration increased the roof and inter-story drift ratios and significantly reduced the base shear capacity leading to early collapse at high levels of deterioration. Recently Dizaj et al.[13] assessed the influence of non-uniform corrosion on the seismic fragility of code-conforming (ductile) and non-conforming (low-ductile) RC frames using a detailed non-linear finite element (FE) model. While the results highlighted the influence of corrosion, it was concluded that consideration of non-uniform corrosion spatial variability has a negligible effect on the global response and seismic fragility of corroded RC frames. Additionally, several researchers have also underlined the impact of corrosion deterioration in RC frame that may be subjected to multiple seismic shocks (multiple mainshocks, or, mainshock-aftershock sequences) along their design life.[14] While the above-mentioned literatures contribute towards the scientific understanding of seismic behavior of aging building structures, these studies do not explore how the corrosion effects influence different failure modes within RC building elements (i.e., shear failure, flexure-shear failure, and flexure failure). This represents a critical aspect in old non-seismically designed (i.e., low-ductile) RC buildings affected by corrosion deterioration.

RC buildings designed before the introduction of modern seismic design codes are often characterized by low-ductility capacity due to insufficient transverse reinforcement in columns and beam-column joints, inadequate anchorage length and hooks for reinforcement, and lap splices in potential plastic-hinge regions of columns, among others.[15] Due to the limited ductility capacity, these buildings are significantly vulnerable to seismic actions. Furthermore, since these structures were constructed before the advent of modern codes, they are presumably aged, and subsequently, corrosion deterioration may further reduce their lateral load-carrying capacity. Within this context, several experimental campaigns have been conducted on RC columns under cyclic loading to identify the negative influence of corrosion on their lateral load-carrying capacity.[16–20] Results from these studies reveal that the flexural strength, energy dissipation capacity, and ductility capacity

of RC columns significantly reduce when the longitudinal reinforcement bars sustain high levels of corrosion. It is worth mentioning that the experimental research listed above only investigated the effects of corrosion on the flexural performance of columns. The tested RC columns were either ductile, or only longitudinal reinforcements were corroded[16,17] and hence predominantly experienced a flexure failure mode. Unlike longitudinal rebars, transverse ties with a thinner concrete cover have a higher disposition toward corrosion effects. Time-dependent deterioration of these shear-resisting reinforcements may lead to unexpected changes in the seismic behavior of the columns. For instance, experimental tests by Vu and Li[21] revealed that 25% corrosion level in transverse reinforcement (stirrups) could reduce the lateral load capacity and alter the failure mechanism from flexure failure to flexure-shear failure under low levels of axial load. For higher axial load levels, the change in failure modes occurs at reduced levels of transverse reinforcement corrosion. In a separate study, Li et al.[22] also reported that with increased corrosion of transverse reinforcement, pure shear failure was observed with considerable loss of strength and stiffness along with pronounced pinching effects. These studies highlight the importance of accounting for the potential flexure-shear and shear failure mechanisms of RC columns in the numerical assessment of the lifetime seismic fragility assessment of aged RC buildings.

Addressing existing drawbacks and augmenting past research, this study presents a framework that aims to assess and quantify the influence of corrosion deterioration on the time-dependent seismic fragility of RC frames using robust numerical models that can capture wide-ranging failure modes of low-ductile RC frames. For confident seismic response predictions, the FE model is validated against available experimental results of the frame and reversed cyclic tests of corroded RC columns having varied failure mechanisms (flexure, flexure-shear, and shear). The present study is performed on a three-story, three-bay RC moment-resisting frame for which laboratory test data on structural performance under dynamic and cyclic loading for the as-built frame exists in the literature. Based on a location-specific exposure condition, a probabilistic model of time-dependent corrosion deterioration of the case-study frame is devised, followed by the development of a state-of-the-art FE model that can capture different failure modes.

While the above investigation on the case-study frame is conducted for an assumed environmental exposure scenario, the proposed framework is extended to derive condition-dependent seismic fragility functions for a generic measure of deterioration (i.e., percentage mass loss of reinforcement area). Such functions offer multiple advantages over traditional techniques to assess the structural vulnerability of a deteriorating structure. Firstly, these functions avert the need for computationally intensive time-history runs to derive fragility estimates for a given exposure. Instead, parametric variation of primary and associated secondary effects of corrosion on building fragility under earthquakes can be assessed directly. Secondly, under an assumed exposure scenario (marine splash/tidal/atmospheric), the theoretical or empirical models available in literature to compute the time-dependent aspects of corrosion are often underlined by several assumptions.[2,23] Furthermore, a majority of these models are based on laboratory tests that may show significant variability from in-situ field conditions leading to non-typical exposure cases. Consequently, the "true" estimate of building fragility may be far removed from the predicted values. The condition-dependent seismic fragility functions proposed in this study help circumvent these challenges and aid building engineers and decision-makers with an easily adoptable model to evaluate seismic fragility given an in-situ building condition.

The subsequent section presents the time-dependent capacity estimates of the case-study frame obtained using nonlinear static analyses for the as-built as well as the corroded frame. Next, non-linear time-history analyses (NLTHAs) results are presented, considering a large set of unscaled natural ground motion records to incorporate record-to-record variability within the seismic response. Comparison of seismic demand and capacity estimates of different damage states (*DSs*) allows the development of seismic fragility curves at different points in time along the service life of the building. Lastly, generic condition-dependent seismic fragility functions are presented to estimate the probability of seismic failure that is independent of a specific exposure scenario and based only on the percentage mass loss measurements. The paper ends with key conclusions and recommendations for future explorations.

2 | FRAMEWORK FOR LIFETIME SEISMIC FRAGILITY ASSESSMENT

Figure 1 shows the overall framework used to evaluate the effects of corrosion on the failure mode and lifetime seismic fragility of low-ductility RC frames. The framework is structured in five Steps (A to E), briefly outlined here and detailed throughout the rest of the paper.

Step A selects a benchmark low-ductility RC frame representative of typical design details prior to the introduction of modern seismic design codes. Past experimental studies on the chosen as-built RC frame highlighted varied failure mechanisms. Additionally, RC members near harsh environmental conditions are prone to aging and deterioration, especially

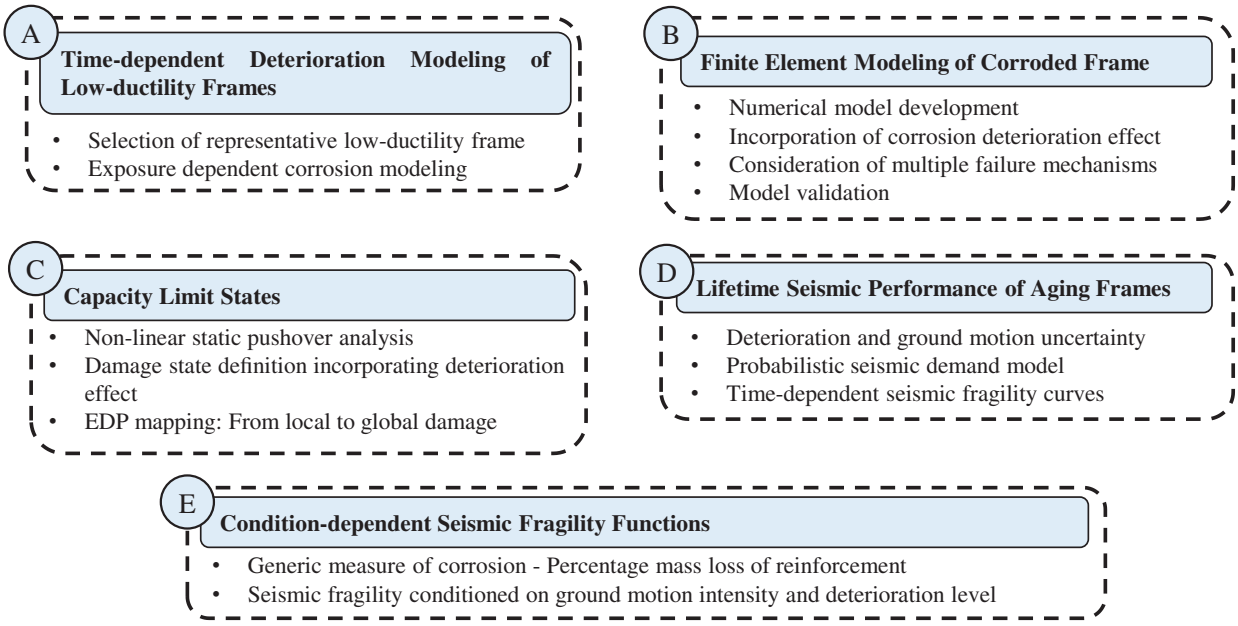

FIGURE 1 Steps of the proposed framework for lifetime seismic fragility assessment of low-ductility corroded RC frames.

when durability considerations were overlooked during the design phase. This may further exacerbate the non-ductile failure modes due to the reduction in both flexure and shear capacities of RC members. This step of the framework also presents a probabilistic corrosion deterioration model for the case-study frame by considering marine environmental exposure conditions while propagating the uncertainty in the deterioration process.

Step B aims at developing a detailed numerical model of the case-study frame incorporating corrosion deterioration effects. The FE model of the as-built frame is based on the previous work of Freddi et al.[15,24,25] and is detailed to capture the varied failure mechanisms that may arise during seismic events. This FE model has been validated against past experimental results at both components and system-level, thereby rendering confidence in the numerical modeling strategy. The corrosion deterioration effects are included in the FE model by incorporating primary and secondary effects of corrosion deterioration, such as area loss of reinforcing steel and changes in mechanical properties of both concrete and steel. The time-dependent parameters of RC columns and beams are calculated based on the deterioration model developed in Step A. The potential alteration in the failure mode of building members due to corrosion is validated in this step with available experimental test results of non-corroded and corroded columns exhibiting varied failure mechanisms (flexure, flexure-shear, and shear).

Step C of the framework aims to map the *DS* thresholds (i.e., the capacity limits) in terms of global engineering demand parameters (*EDPs*) for uncorroded as well as corroded frames at different points in time along their service life. The use of global *EDPs* has several advantages, and, amongst others, they synthetically describe the structural response containing the computational effort involved in the analysis of complex models. Alternative strategies include the definition of the *DSs* of the structure directly considering local *EDPs* at member and/or section-level, for example, rotation, strength of cross-sections, and material strains[24–28] or the use of *DS* thresholds adopted from standard guidelines.[29] However, the direct use of local *EDPs* is usually too computationally demanding, while the use of code-based *DS*s for low-ductile non-seismically designed RC frames may lead to under-prediction of failure probability, in particular when the considered structure is undergoing material aging and time-dependent structural degradation. Consequently, Step C develops structure- and corrosion-dependent *DS* thresholds for the case-study RC frame using non-linear static pushover analyses wherein global *EDPs* are mapped based on local *EDPs*.[15,30] These *DS* thresholds for the considered global *EDP*, that is, the maximum inter-story drift ratio (IDR_{max}), are based on local-level *EDPs* (i.e., material strains in beams and columns) while also accounting for local mechanisms directly in the model, such as shear failure of columns.

Step D develops time-dependent seismic fragility curves for the aging RC frame while accounting for the uncertainties related to corrosion deterioration and ground motion record-to-record variability. At a particular point in time along the design service life (considered as 50 years for residential building), these fragility curves represent conditional probabilistic statements for meeting or exceeding a specific *DS* threshold given the ground motion intensity measure

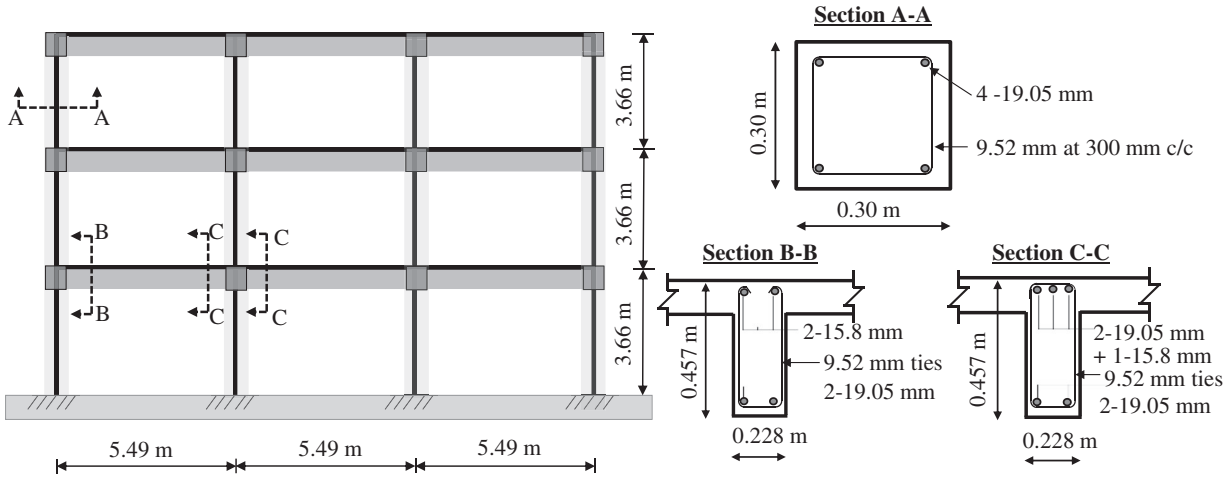

FIGURE 2 Case-study frame (adapted from Bracci et al.[34] and Aycardi et al.[36]).

(*IM*).[7,31] The time-dependent seismic fragility curves are developed using a two-phase approach. First, probabilistic seismic demand models (PSDMs) are developed using non-linear time-history analyses of corroded RC frame models at different time intervals. Next, a suite of unscaled earthquake ground motions is used for NLTHAs such that the structure experiences behavior ranging from the linear to the non-linear domain, thereby covering the different *DS* definitions. These PSDMs provide a one-to-one relationship between a selected *EDP*, such as the IDR_{max}, and the ground motion *IM*.[31] The second phase involves the development of time-dependent seismic fragility curves using the PSDMs and *DS* thresholds. These time-dependent seismic fragility curves help evaluate the probability of damage due to seismic shaking at different points in time along with the structure's service life.

Since the corrosion deterioration mechanism in nature is substantially uncertain and dependent on in-situ field conditions, the observed extent of structural degradation may often deviate from corrosion model predictions for typical exposure scenarios. Thus, in addition to seismic fragility assessment for chosen marine exposure conditions, Step E of the framework also proposes condition-dependent seismic fragility functions. These flexible fragility functions are conditioned on generic measures of corrosion, such as the percentage mass loss of steel. A seismic fragility surface is developed for the case-study RC frame conditioned upon the extent of deterioration (percentage mass loss of steel) and ground motion intensity. Development of the fragility surface leads to easy adoptability of the research results by engineers, building owners, and decision-makers to estimate failure probability based on the in-situ deterioration level. A detailed description of Steps A to E is reported in Sections 3–6 of the paper.

3 | LOW-DUCTILITY RC FRAME: DESCRIPTION OF CASE-STUDY FRAME, CORROSION DETERIORATION, AND FINITE ELEMENT MODELING

The impact of corrosion deterioration on the lifetime seismic fragility of the RC frame is demonstrated on a representative case-study RC frame assumed to be located in the coastal region of California, US. The case-study frame is non-seismically designed (i.e., low-ductility) and representative of typical construction practices in several areas of the US as well as similar earthquake-prone regions in Europe and Asia prior to the introduction of modern seismic design codes. In addition to the seismic hazard threats, corrosion deterioration significantly effects the load-carrying capacity of these low-ductility buildings which may lead to precarious brittle failure modes during earthquakes.[32,33]

3.1 | Description of the case-study frame

Figure 2 shows the layout of the selected case-study frame, which has been adopted from Bracci et al.[34] The selected three-story, three-bay RC moment-resisting frame is representative of non-seismically designed (i.e., low-ductility) low-rise RC buildings. The frame has a total height of 10.75 m (35.3 feet) with an inter-story height of 3.66 m (12 feet) and a constant bay width equal to 5.49 m (18 feet). The building frame is designed for gravity loads only, following the pre-seismic design

provisions of ACI 318−89.[35] The column sizes are 300 × 300 mm, and the beam sizes are 230 × 460 mm at each floor. The concrete design compressive strength is 24 MPa, and the longitudinal reinforcing bar of steel Grade 40 has a yield strength of 276 MPa. The reinforcement details of the case-study frame, as shown in Figure 2, are adopted from Bracci et al.[34] and Aycardi et al.[36] Reinforcement details from these studies reveal that the columns and beam-column joints have insufficient transverse reinforcement, inadequate anchorage length and hooks for reinforcement, and lap splices in potential plastic-hinge regions.

3.2 | Time-dependent deterioration modeling of the case-study frame

When located in adverse environmental conditions, RC buildings are subjected to time-dependent aging and degradation. The aging and deterioration process of RC structures manifests in the form of corrosion and other physical and chemical degradation processes. Among these, corrosion deterioration due to the ingress of chloride ions constitutes a dominant form of degradation of RC structures.[8,37,38] Sources of chlorides may stem from marine environments or airborne chlorides that constitute common exposure scenarios for RC buildings located in the coastal area of the case-study region of California.[39] Accordingly, this study considers chloride-induced corrosion as the primary form of time-dependent degradation of the case-study building frame, with the chosen exposure scenario indicative of high deterioration levels.[40,41]

Corrosion deterioration in RC structures begins after a time interval known as the corrosion initiation time (T_{init}), wherein the chloride ions gradually penetrate the concrete cover, depassivates the reinforcing steel, and initiates corrosion. This study uses the widely adopted probabilistic model proposed by Duracrete[42] to predict corrosion initiation time as:

$$T_{init} = X_t \left\{ \frac{{c_v}^2}{4k_e k_c k_t D_{cl,0}(t_0)^{n_{cl}}} \left[erf^{-1}\left(\frac{C_s - C_{cr}}{C_s}\right)\right]^{-2} \right\}^{\frac{1}{(1-n_{cl})}} \tag{1}$$

where, c_v is the concrete cover depth in mm, $D_{cl,0}$ is the diffusion coefficient at $t_0 = 28$ days in mm^2/year (determined from the compliance tests), k_t is the correction factor of tests performed to estimate $D_{cl,0}$, k_e, and k_c are the environmental and curing factor, X_t is the modeling uncertainty factor, n_{cl} is the age exponent considering densification of cement paste due to hydration chloride, C_s is the equilibrium chloride concentration at the exposed concrete surface, C_{cr} is the critical chloride concentration, and *erf* is the Gaussian error function. Table 1 shows the probabilistic distribution of the parameters to estimate corrosion initiation time.[42]

Considering the probabilistic distribution of the above-mentioned parameters (Table 1), a Monte Carlo simulation is carried out to estimate the mean corrosion initiation time for longitudinal and transverse reinforcement of RC members. It may be noted that the variables used to evaluate the time to corrosion initiation and eventual propagation (Table 1) are assumed to be statistically independent. Following 10,000 Monte Carlo trials, a lognormal distribution is deemed appropriate to represent the statistics of the corrosion initiation time. A lognormal distribution with a mean of 10 years is found to be a good fit to the simulated data for corrosion initiation time of transverse steel reinforcement, having a mean cover depth of 38.1 mm. Figure 3A shows an overlay of the empirical CDF of the Monte Carlo trials and the fitted lognormal distribution for transverse steel reinforcement. Similarly, the mean corrosion initiation time for longitudinal steel reinforcement is estimated as 14 years. Note that a lower initiation time is expected for transverse steel compared to longitudinal reinforcement due to the reduced concrete cover (see column details in Figure 2).[43]

Following the initiation phase, the corrosion propagation phase is marked by the formation of small independent pits or cracks along the steel rebar that, with time, lead to wider cracks resulting in uniform corrosion.[2] The cross-sectional area of reinforcing steel at time t [$A_{st}(t)$] can be estimated as:

$$A_{st}(t) = \begin{cases} \frac{\pi}{4}[\phi_0]^2 & for\ t \le T_{init} \\ \frac{\pi}{4}[\phi_0 - 0.0232 \times i_{corr} \times t]^2 & for\ t > T_{init} \end{cases} \tag{2}$$

where, ϕ_0 is the diameter of the uncorroded reinforcing steel, t is the elapsed time, T_{init} is the corrosion initiation time [Equation (1)] in years, i_{corr} is the corrosion current density in μA/cm^2, and 0.0232 is the conversion factor of corrosion rate from μA/cm^2 to mm/year. While several corrosion rate models are available in literature,[1,44,45] to maintain consistency

TABLE 1 Probability distribution of the parameters involved to estimate corrosion initiation time and rate of corrosion deterioration.[42]

$D_{cl,0}$: Reference chloride diffusion coefficient for w/c ratio = 0.50				
Distribution: $N(\mu, \sigma)$[a]	μ		σ	
	473.0 mm^2/year		43.2×10^{-12} m^2/s	
k_e: Environmental correction factor				
Distribution: *Gamma* (α, β)[b]	α		β	
	2.92		11.0	
k_c: Correction factor for curing time (At age 7 days)				
Distribution: Beta (a, b, p, q)[c]	a	b	p	q
	1.0	4.0	2.15	10.7
k_t: Correction factor for tests[42]				
Distribution: $N(\mu, \sigma)$	μ		σ	
	0.832		0.024	
n_{cl}: Aging factor or age exponent[42]				
Distribution: Beta (a, b, p, q)	a	b	p	q
	0.0	1.0	17.2	29.3
C_{cr}: Critical chloride concentration (% relative to binder)				
Distribution: $N(\mu, \sigma)$	μ		σ	
	0.50		0.10	
C_s: Surface chloride concentration (% relative to binder)[42]				
$C_s = A_{cs}(w/b) + \varepsilon_{cs}$, where w/b is the water-binder ratio (assumed as 0.5 in this study), A_{cs} is the chloride surface content regression parameter, and ε_{cs} is the error term for surface chloride concentration.				
A_{cs}: Chloride surface content regression parameter (% relative to binder)				
Distribution: $N(\mu, \sigma)$	μ		σ	
	7.76		1.36	
ε_{cs}: Chloride surface content error term				
Distribution: $N(\mu, \sigma)$	μ		σ	
	0		1.11	
X_t : Modeling uncertainty factor				
Distribution: $LN(\lambda, \zeta)$[d]	λ		ζ	
	−0.0012		0.05	
c_v: Concrete cover depth (mm)				
Distribution: $LN(\lambda, \zeta)$	λ		ζ	
	3.62 for transverse steel, and 3.84 for longitudinal steel		0.20	
i_{corr}: Corrosion rate ($\mu A/cm^2$)				
Distribution: $LN(\lambda, \zeta)$	λ		ζ	
	0.766		0.60	

[a] $N(\mu, \sigma)$ refers to Normal distribution with μ and σ representing the mean and standard deviation.
[b] Gamma (α, β) refers to Gamma distribution with shape parameter α and inverse scale parameter β.
[c] Beta (a, b, p, q) refers to a four-parameter Beta distribution with a and b representing the upper and lower bounds, and p and q representing the shape parameters.
[d] $LN(\lambda, \zeta)$ refers to Lognormal distribution with λ representing ln(median) and ζ representing lognormal standard deviation.

with the corrosion initiation model, the corrosion rate is also adopted from Duracrete[42] and reported in Table 1. Note that non-uniform pitting corrosion of steel reinforcement is not studied in this work for the sake of simplicity. However, based on the recommendations of Dizaj et al.,[13] the effects of non-uniform pitting corrosion, such as the reduction in steel strength and ductility, are explicitly included, as elaborated later. Figure 3B shows the variation of mean reinforcing steel area (longitudinal and transverse) with time, along with the lower and upper limits of the uncertainty band representing the 5th and 95th percentile confidence bounds after incorporating the uncertainties in the corrosion deterioration process. The effect of area loss of reinforcement is more pronounced for smaller diameters[46]; thus, a higher percentage of area loss

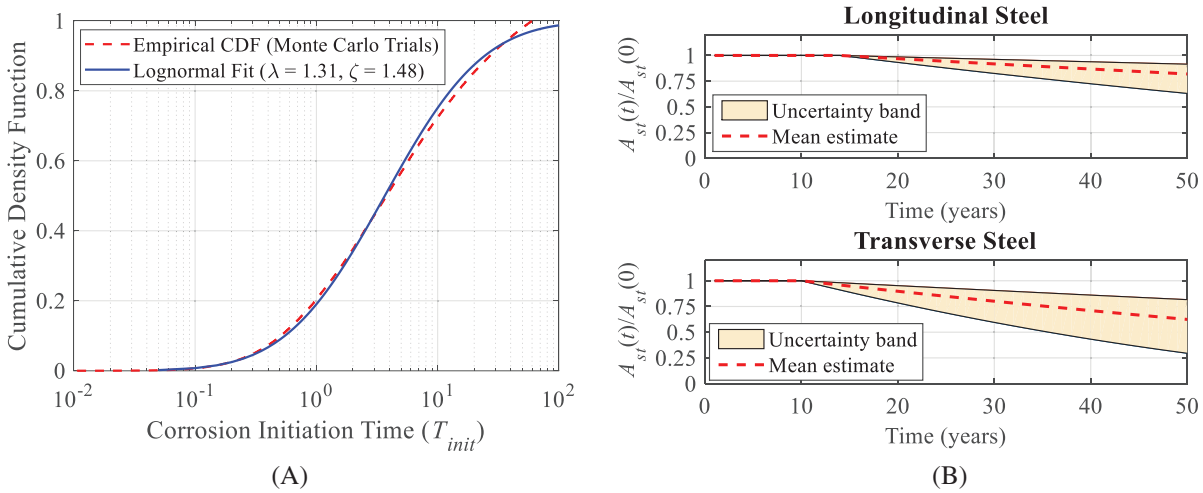

FIGURE 3 (A) Empirical cumulative distribution along with the lognormal fit for the corrosion initiation time for transverse reinforcement (cover 38.1 mm) and (B) variation of mean longitudinal and transverse steel area with time along with the lower and upper limits (5th and 95th percentile) of the uncertainty band.

is observed for transverse steel, as evident in the figure. At the end of 50 years, 19% and 38% reduction in area loss can be observed for longitudinal and transverse reinforcement of columns, signifying the necessity of considering corrosion deterioration in the lifetime seismic fragility assessment of RC buildings. In addition to the primary effect of corrosion deterioration through area loss of longitudinal and transverse reinforcements, the present study also considers several secondary effects, such as the reduction in concrete core and cover strength and in steel strength and ductility. This is elaborated on next.

Expansive rust products formed due to rebar corrosion result in the generation of micro-cracks that can lead to a reduction in cover concrete strength and even spalling of concrete over time. The deterioration of concrete cover strength is evaluated using the model proposed by Coronelli and Gambarova.[47] The concrete core strength is a function of the volumetric ratio of transverse reinforcement (stirrups) and undergoes a time-dependent reduction due to corrosion deterioration. This time-dependent loss in core concrete strength can be estimated based on the modified theoretical stress-strain model proposed by Mander et al.[48] However, for the case-study frame due to wide spacing of stirrups (300 mm), decrease in core concrete strength caused by stirrup corrosion is minimal. Reduction in steel mechanical properties due to corrosion deterioration along the rebar length is manifested through changes in yield strength, ultimate strength, and ultimate strain. This study utilizes the time-dependent empirical model proposed by Du et al.[49] for steel strength reduction, wherein the yield and ultimate strength decrease linearly with mass loss. Note that for uniform corrosion (as adopted in this study), the mass loss over the length of the reinforcement is equivalent to the area/section loss of the reinforcement. The ultimate strain reduction in steel, however, does not follow a linear reduction, as past research revealed that strain reduction values are scattered over a large range.[50] As a result, this research incorporates experimental findings reported by Apostolopoulos and Papadakis,[51] which implies a non-linear reduction in ultimate strain with a percentage mass loss of reinforcing steel. Note that unlike empirical relationships that are derived from experimental test results of corroded rebars, recent techniques such as digital image correlation,[52] provide a better estimate for the reduction in mechanical properties of steel. The reduction in shear strength of RC columns due to corrosion of transverse reinforcements can contribute to the potential of flexural failure modalities translating to flexure-shear or shear failures. The time-dependent shear strength loss of RC column is calculated based on the model proposed by Vu and Li,[21] that takes into account various member characteristics such as the compressive strength of concrete, aspect ratio, core and cover concrete area, transverse steel reinforcement area and yield strength, and axial load on the member. At the end of its service life (i.e., 50 years), the deteriorated RC columns also undergo 79%, 10%, 67%, and 25% mean reduction in the concrete cover strength, steel strength, ultimate steel strain, and shear strength, respectively (Figure 4), signifying the need to consider these secondary effects in the lifetime performance assessment of RC frame buildings. Note that for the sake of clarity, uncertainty bands (5th and 95th percentile confidence bounds) around the mean estimates are not shown in Figure 4.

In addition to the above secondary effects, corrosion deterioration in RC columns may also result in bond strength reduction, buckling strength reduction, and low-cycle fatigue degradation, among others.[53,54] The reduction in bond strength

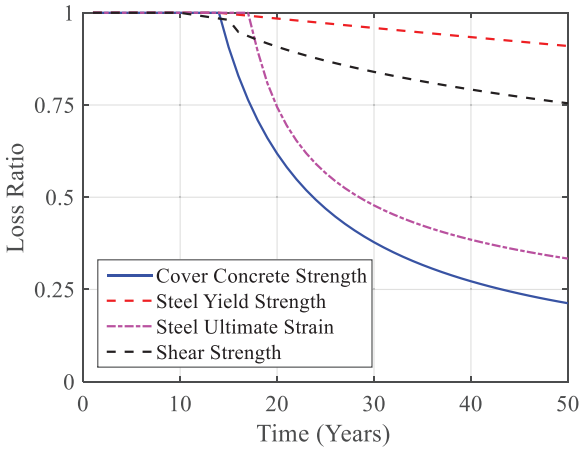

FIGURE 4 Time-dependent variation of the mean values of concrete cover strength, steel strength, ultimate strain, and shear strength of RC columns.

of RC members due to corrosion is negligible for modestly confined RC members with transverse reinforcement, as is the case in the case-study frame RC columns.[55,56] Moreover, researchers also demonstrated that bond strength reduction has minimal influence on the failure probability of corroded structure under cyclic loading,[53,54,57] consequently this effect is neglected. For rebar buckling, a preliminary investigation by authors for the case-study frame showed that rebar buckling strain of 0.06, as suggested by Kowalsky,[58] is attained after the shear failure initiation in the RC columns. Therefore, rebar buckling effect is not explicitly modeled in the present study. It is important to note that phenomenological uniaxial material model for corroded reinforcing steel bars accounting for inelastic buckling and low-cycle fatigue degradation are available in the literature.[59,60] These models can be explored in the future for RC columns susceptible to rebar buckling.

3.3 | Finite element modeling of the case-study frame

A two-dimensional high-fidelity FE model of the case-study frame is developed in OpenSees.[61] The FE modeling strategy for the case-study frame follows the approach presented by Freddi et al.,[15] which focuses on simulating the global response of the system as well as the local seismic response of structural components, including brittle failure mechanisms—typical of low-ductility RC moment resisting frames. This modeling strategy enables capturing local failure mechanisms that, in turn, aid in monitoring the influence of corrosion deterioration of building components on the global response parameters.

3.3.1 | Finite element modeling of the case-study frame incorporating corrosion deterioration effects

Figure 5 shows the schematic representation of the FE model, highlighting modeling details of different structural components such as beam and column sections, interior and exterior beam-column joints, and shear springs. The non-linear flexural response of columns is captured using the *nonLinearBeamColumn* element that is based on distributed plasticity approach. The column section is modeled using a fiber section that includes cover and core concrete patches and layers of reinforcement (Figure 5). Both the unconfined concrete cover and the confined concrete core are modeled using *Concrete02* material. The confined concrete parameters are calculated based on Mander et al.[48] Steel reinforcements are modeled using the *Hysteretic* material, which allows for capturing pinching of force and deformation, damage due to ductility and energy, and degraded unloading stiffness based on ductility. Calibrating the hysteretic material model in OpenSees to reproduce pinching behavior allows for a more accurate simulation of the structural response, and therefore, based on the experimental result of Aycardi et al.,[36] the Hysteretic material pinching, strength, and stiffness degradation parameters are calibrated for the case-study as-built frame columns. Beams are modeled using the *beamWithHinges*

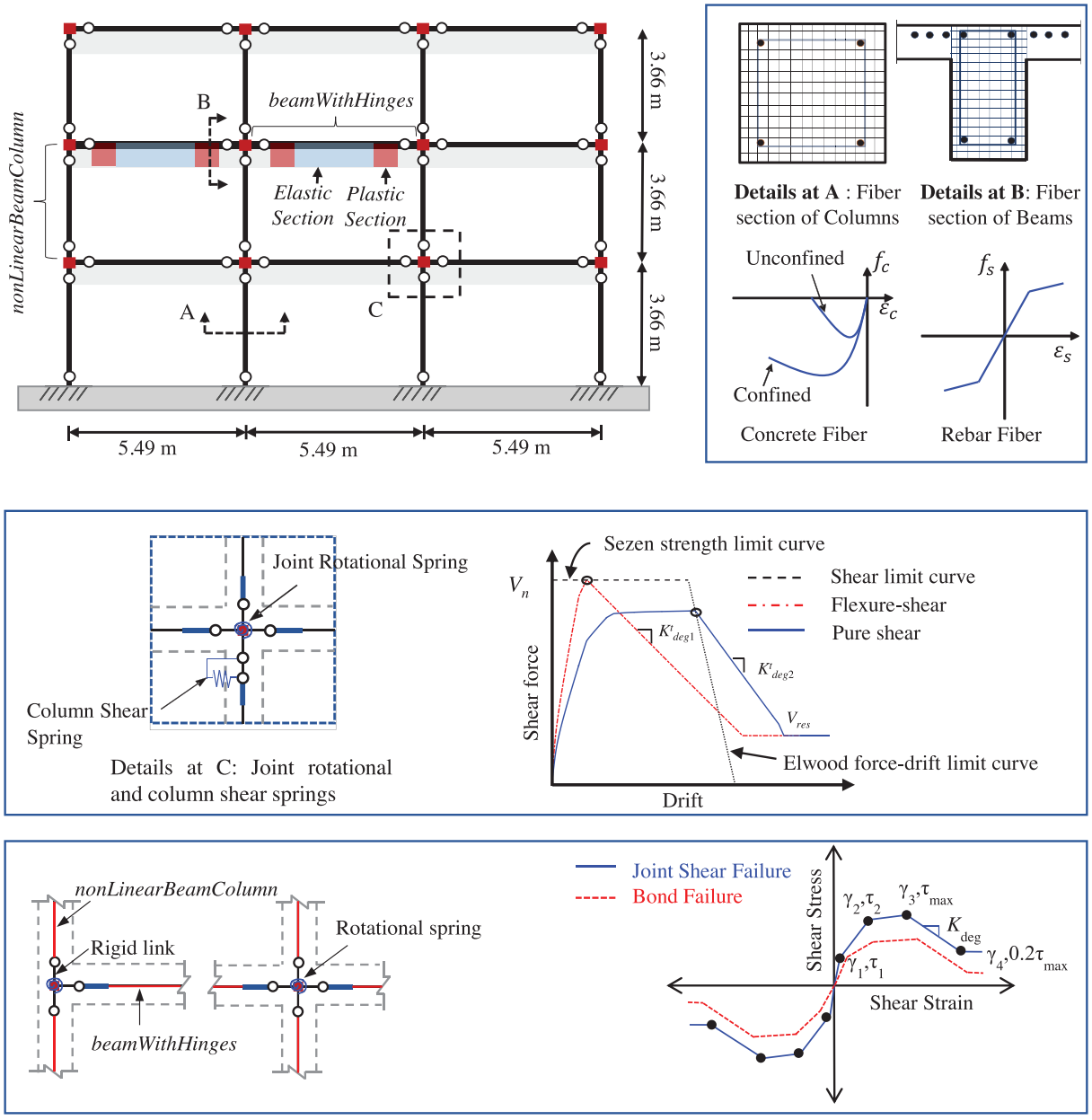

FIGURE 5 Overview of the numerical modeling strategy for the case-study frame.

element that consists of a central elastic element and two plastic hinge regions at the element ends defined by fiber sections. The plastic hinge of beams is evaluated based on the model proposed by Panagiotakos and Fardis,[62] and fiber sections are defined similarly to the approach adopted in columns. The slab is modeled using the unconfined concrete material model with an effective width equal to four times the width of the beam.[35] Gravity loads are distributed on the beams, while masses are concentrated at the beam-column intersections.

The study considers an external bay frame, and the effect of corrosion is assumed to be uniformly distributed around the perimeter of beams and columns, with all stories undergoing the same level of deterioration. It is noteworthy that this study considers the worst-case scenario to assess the influence of corrosion deterioration on failure modes and seismic vulnerability. However, further analyses are required to address more realistic scenarios. These scenarios should differentiate the corrosion effects in internal and external frames, account for the presence of infills, which could potentially safeguard the RC members from corrosion, and explicitly consider the presence of the slabs which protect the upper side of the beams from corrosion, resulting in a non-uniform distribution of corrosion within the structural elements. For the deteriorated RC beams and columns, the consequences of chloride-induced corrosion, such as area loss of steel

and various secondary effects previously outlined in Section 3.2, are incorporated along with the associated uncertainties. The area loss of steel due to corrosion is modeled as a uniform reduction in rebar diameter along the circumference and includes the corrosion rate time-dependent uncertainty (Table 1 and Figure 3). The FE modeling of the degraded frame also includes the outlined secondary effects of corrosion deterioration, such as rebar strength and ductility loss, as well as loss of cover and core concrete strength (Figure 4). In the corroded frame, the loss of strength and ductility of rebars is captured by calculating the time-dependent reduction, and updating the parameters of the *Hysteretic* material. The core concrete strength reduction due to corrosion of transverse reinforcement and loss of cover strength due to the formation of expansive rust products is incorporated in the corroded frame by updating the parameters of *Concrete02* material.

While the above fiber section-based modeling of RC sections is capable of capturing the non-linear flexural deformation, non-seismically designed low-ductility frames may also exhibit non-linear behavior due to column shear failure and loss of gravity load-bearing capability.[63] Consequently, a zero-length shear spring (element *zeroLength* in OpenSees) is placed in series with the column flexure element, as shown in Figure 5. The *uniaxial LimitState* material model is assigned to these springs that monitor columns response and "triggers" only when the column response reaches the pre-defined shear limit curves (implemented within OpenSees as *limitCurve Shear*). Note that the existing *limitCurve Shear* model is modified such that shear failure may occur when the column response reaches either the strength or drift limit curves.[15,64] While the shear strength limit curve is based on the model proposed in ASCE-41, the deformation limit curve is defined based on an empirically derived force-deformation controlled limit curve given by Elwood.[63] Both strength and drift shear limit curves depend on parameters such as column transverse reinforcement, column axial load, section dimensions, and material properties, among others, and therefore, are affected by the level of column corrosion. The considered FE modeling approach considers this degradation of shear limit curves during the non-linear analysis. The degrading slope of the total response ($K^t{}_{deg}$ in Figure 5) is calculated using the shear-friction model proposed by Baradaran-Shoraka and Elwood.[65] The degrading stiffness of the shear spring response (K_{deg} in Figure 5) is estimated from the degrading slope of the total response $K^t{}_{deg}$ and the unloading stiffness of the flexural response (K_{unload}).[63] Also, the residual strength is defined as 20% of the nominal shear strength to alleviate potential convergence issues in OpenSees.[33]

To model the low-ductility joints for the RC frame, a two-node *zeroLength* rotational joint spring, and four rigid offsets are used, as done by Jeon et al.[33] and shown in Figure 5. In this model, beams and columns are continuous, while the joint model controls their relative rotation. Joint failures could be related to insufficient traverse reinforcement and short embedded reinforcement lengths within the beam-column joints. To account for the short anchorage length, a reduced shear strength is considered, as suggested by Jeon et al.[33] Also, to account for the pinching behavior, the *Pinching4* material model[61] is used for the beam-column joint response, as shown in Figure 5. Lastly, the present study does not consider the influence of corrosion deterioration on the behavior of joints. A recent study by Zhang and Li[66] highlights that such effects are more significant for axial load ratios greater than 0.20. A preliminary investigation by the authors revealed that the average axial load ratios for exterior and interior joints of the case-study frame are approximately 0.05 and 0.13, respectively. Therefore, the effect of corrosion on joint stresses is currently neglected and will be investigated in the future based on the availability of additional experimental tests on corroded joints.

3.3.2 | Validation of the finite element model against experimental results

The numerical model of the as-built case-study frame is validated at component- and system-level using the experimental response data of the 1:3 scaled model of columns, beam-column subassemblages, and overall frame from Aycardi et al.[36] and Bracci et al.[34] At both component and system levels, the numerical model results show a close match with the experimental results. These validation results are similar to those reported by Freddi et al.,[15,24] and for the sake of brevity, are not reported herein. For the considered case study structure, the experimental tests of the as-built frame did not indicate pure shear or flexure-shear failure of columns under cyclic loading or with the ground motion intensities used during the shaking table tests. However, corrosion of RC columns could lead to a transition in the failure mode from flexure to flexure-shear or shear. Consequently, the numerical modeling approach of RC columns is validated using the experimental results of four uncorroded and corroded RC column specimens in the literature that exhibit different failure mechanisms. Appendix A details the specimens used for the validation.

Figure 6A,B show the comparison of analytical responses with the experimental results of two uncorroded RC columns, that is, Specimen 1 from Sezen[67] and Specimen 19 from Ghee et al.[68] These specimens exhibit respectively flexure-shear and shear failures due to widely spaced transverse reinforcements. It is observed that the numerical model satisfactorily predicts the experimental response in terms of maximum shear force, energy dissipation, and normalized hysteretic

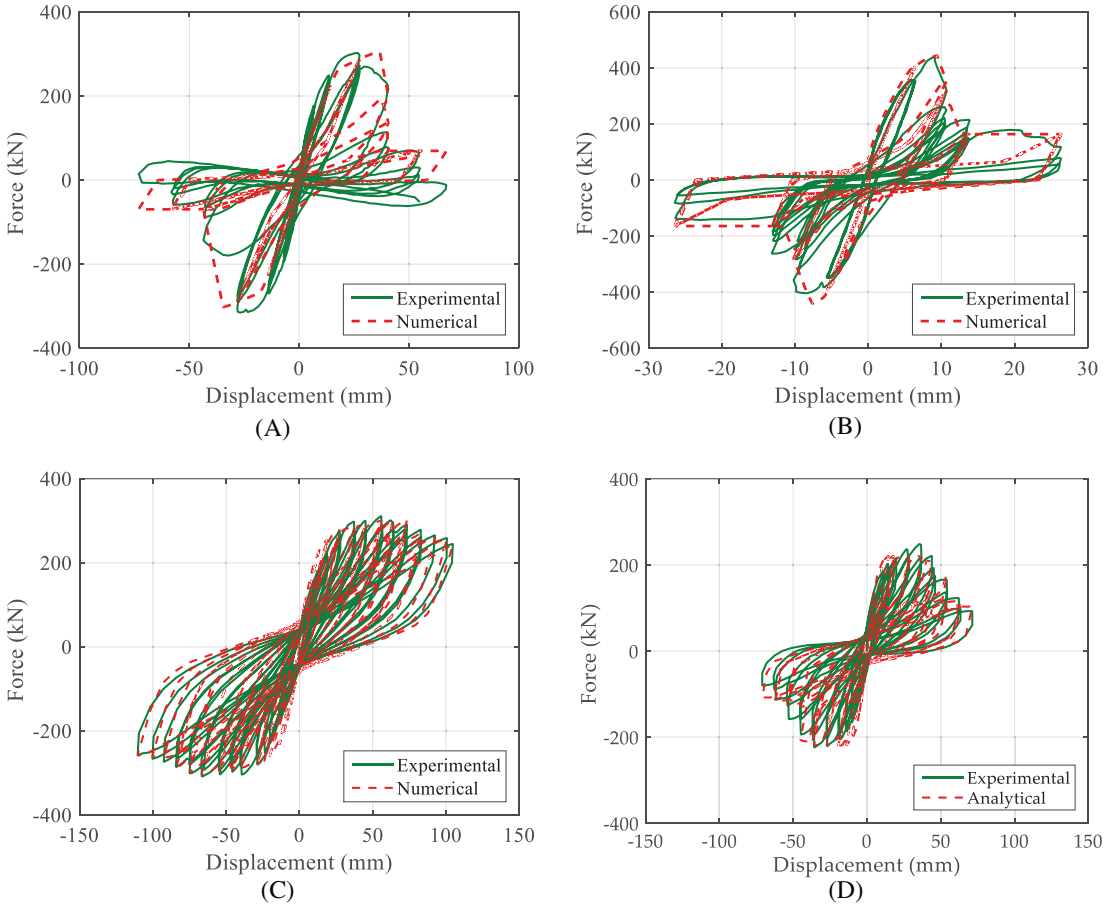

FIGURE 6 Comparison of experimental and numerical response for (A) Uncorroded flexure-shear critical column, Specimen 1,[67] (B) Uncorroded shear critical column, Specimen 19,[68] (C) Uncorroded flexure critical column, Specimen U2,[21] and (D) Corroded flexure-shear critical column, Specimen C5.[21]

force while reasonably capturing the strength and stiffness degradation. Also, to further emphasize the capability of the numerical modeling approach to capture change in failure mechanisms due to corrosion deterioration, two additional RC column specimens are chosen from the literature, that is, Specimen U2 and C5 from Vu and Li.[21] While these two specimens have the same structural and geometrical characteristics (Table A1), there is a noticeable shift in failure mechanisms due to reinforcement corrosion. While the uncorroded specimen U2 experienced flexure failure, the corroded specimen C5 failed in shear due to corrosion of longitudinal and transverse reinforcements. Figure 6C,D compare the simulated and experimental lateral force-displacement curves of the two specimens. It can be observed that overall, the proposed model can simulate the hysteretic behaviors of both uncorroded and corroded columns reasonably well and capture the change of failure mechanism from flexure to flexure-shear due to the corrosion of reinforcements. The numerical model also satisfactorily predicts the reduction in maximum shear force due to corrosion.

4 | TIME-VARYING CAPACITY ESTIMATION OF CORRODED LOW-DUCTILITY FRAME

Seismic fragility assessment of building structures is a typical demand-capacity problem that involves the seismic demand assessment using NLTHAs, and comparison against respective capacity estimates of different *DSs*—such as Slight, Moderate, Extensive, and Complete.[29] The time-varying structural characteristics related to corrosion-induced aging affect the lateral load-resisting capacity of the building structure. Hence, this part of the study estimates the time-evolving distribution of *DS* thresholds for the case-study deteriorating RC frame using non-linear static analyses. Structure-specific capacity limits in terms of IDR_{max} thresholds for the four *DSs* are calibrated via non-linear static analysis with a load distribution

TABLE 2 Damage states (*DSs*) description and *DSs* thresholds mapping.

Damage states	Description	*DS* thresholds: IDR_{max} (%)					
		As-built		25-year		50-year	
		C_{med}	β_c	C_{med}	β_c	C_{med}	β_c
Slight	Yielding of 50% of columns at one story	0.690	0.350	0.664	0.354	0.555	0.360
Moderate	Crushing/spalling of concrete in 50% of columns at one story	1.240	0.350	1.103	0.355	0.714	0.410
Extensive	Average of moderate and complete *DSs*	2.110	0.350	1.796	0.357	1.482	0.362
Complete	Initiation of shear failure in 50% of columns at one story	2.970	0.350	2.474	0.363	2.252	0.348

Note: C_{med} and β_c are the median and lognormal standard deviation estimates of *DS* capacity thresholds.

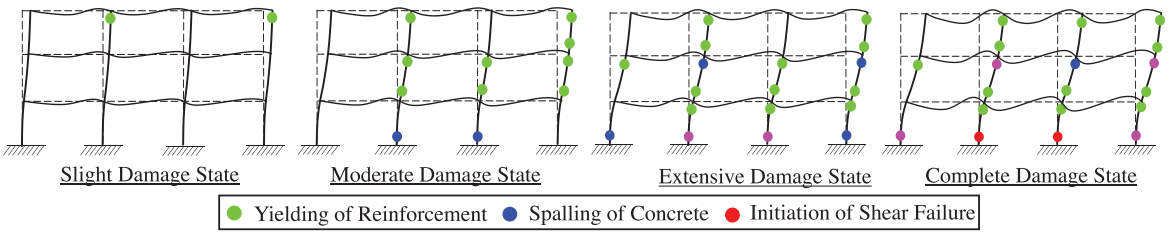

FIGURE 7 Deformed shape of the as-built frame at various damage states with markers showing attainment of failure criteria.

according to the first vibration mode by assessing multiple measurable criteria.[30,69] Table 2 lists the qualitative physical description of building damage associated with each of the *DSs*. The Slight *DS* corresponds to yielding of columns and is quantitatively defined as the IDR_{max} when 50% of columns at one story yields. The Moderate *DS* corresponds to crushing or spalling of concrete in columns and is quantitatively defined as the IDR_{max} when spalling strain reaches a value of 0.004 in 50% of columns at one story. The Complete *DS* corresponds to the initiation of shear failure in 50% of columns at one story. The IDR_{max} for the Extensive *DS* is assumed as the average of IDR_{max} corresponding to Moderate and Complete *DSs*.

Figure 7 shows the deformed shape of the as-built frame for various *DS*s. The figure also illustrates the location within the frame where the threshold criteria for each *DS* are attained. As evident from the figure, the initial yielding (Slight *DS*) first takes place at the two top story columns, indicated by a green marker in the deformed shape. The Moderate *DS* is attained when two columns from the ground story reach the spalling strain limit, denoted by a blue marker. It is worth noting that once the Moderate *DS* is reached, yielding also occurs in additional columns, indicated by green marker. The Complete *DS* (initiation of shear failure in 50% of columns at one story) occurs first in the ground story columns, indicated by a red marker. Although not shown here, similar deformed shapes are also observed for the 25- and 50-year corroded frames. Note that the IDR_{max} corresponding to various *DSs* are noted and mapped in the global base shear versus IDR_{max} plot of as-built RC frame as shown in Figure 8A. This figure also shows the base shear versus IDR_{max} plot for frame at 25-year, and 50-year of service life considering the mean value of deterioration parameters. The figure also shows the markers corresponding to the attainment of different *DSs*. The detrimental effects of corrosion deterioration led to reductions in load-carrying capacity due to section loss of steel and several secondary effects of corrosion, as mentioned earlier. Compared to the as-built frame, corrosion deterioration at 50 years results in approximately 25% reduction in base shear capacity. Analogous to reduced load carrying capacity, IDR_{max} limit corresponding to different *DSs* also show a decreasing trend.

Lastly, a Monte Carlo approach is used to find the probability distribution for each *DS*.[70,71] Based on the uncertainty in deterioration parameters (described in Section 3.2), at different points in time along the service life (25- and 50-year), 5000 random RC frame samples are generated by considering 100% correlation across the different structural elements (beams and columns). In other words, all beams and columns within the case-study structure are assumed to deteriorate similarly once exposed to environmental chlorides. This is an approximation and can be improved by considering spatial correlation between the building elements.[72] Non-linear static analyses are conducted on these RC frame samples recording the different *DSs*. Since the adopted Monte Carlo approach only accounts for uncertainty stemming from deterioration parameters, the epistemic uncertainty stemming from lack of knowledge, modeling assumptions, or construction quality is accounted for by considering an additional lognormal standard deviation of 0.35.[70,73] Following Monte Carlo trials, lognormal distributions emerge as the best fit for the data for each *DS*. Figure 8B shows an example of lognormal fit to the

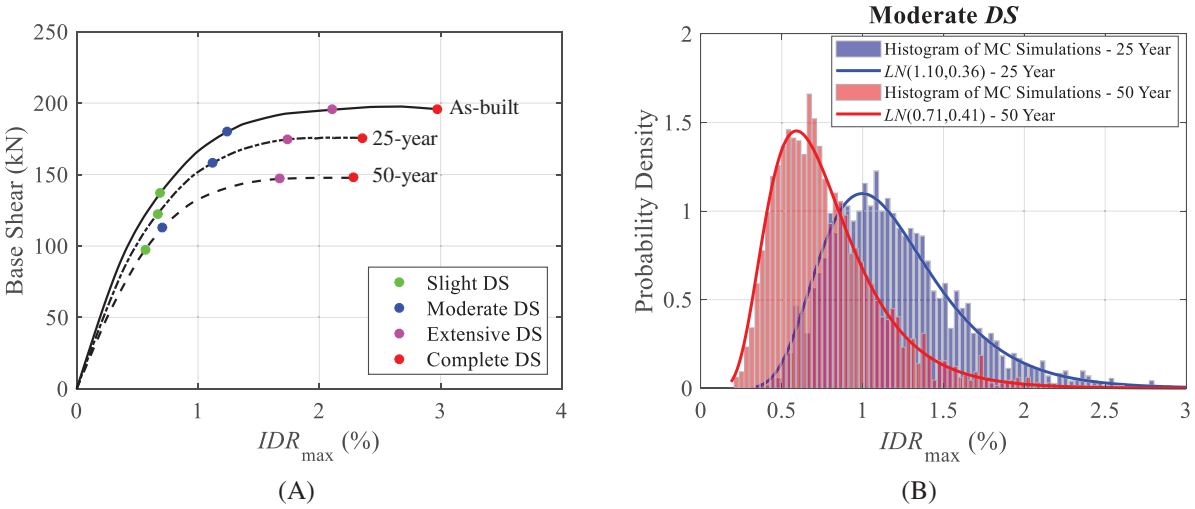

FIGURE 8 (A) Non-linear static analysis results for as-built and deteriorated frames showing Base shear versus IDR_{max} curves and mapping of IDR_{max} values with *DSs* thresholds and (B) probability density functions for the Moderate *DS* accounting for corrosion modeling uncertainty.

$IDR_{\max}$ obtained from Monte Carlo simulation based non-linear static analyses for the Moderate damage state of the 25- and 50-year RC frames. Table 2 shows the complete list of the median (C_{med}) and dispersion (β_C) of each *DS* of the RC frame at different points in time, along with the service life (i.e., as-built, 25, and 50-year). The median $IDR_{\max}$ of 50-year frame for Slight, Moderate, Extensive, and Complete *DSs* are 19%, 43%, 30%, and 24% lower as compared to *DSs* of as-built frame.

5 | TIME-DEPENDENT SEISMIC FRAGILITY FUNCTIONS

This part of the study develops time-dependent seismic fragility curves for the four different *DSs* along with the service life of the structure. At a given point in time, these curves are developed after comparing the seismic demand and capacities of nominally similar but statistically different FE frame models. These models reflect the deterioration uncertainty pertaining to corrosion degradation of the frame. Seismic fragility curves are developed for the as-built, 25-year, and 50-year frames using the Cloud Analysis approach[31] that utilizes PSDMs and *DS* thresholds derived in Section 4, as illustrated in Step D of the framework (Figure 1).

5.1 | Ground motion selection

This study utilizes a set of 150 unscaled ground motion records to carry out NLTHAs of the as-built and deteriorated building frame models and subsequently develop time-dependent seismic fragility curves. These 150 ground motions are adopted from the SIMBAD database,[74] consisting of a total of 467 tri-axial accelerograms produced by 130 earthquake events across the globe. The database includes shallow crustal earthquake records with moment magnitudes ranging from 5 to 7.3 and epicenter distances less than 35 km. In this database, most of the records are representative of soil type B (44%) and C (43%), while only a few of them are recorded on rock (8%), or soft soils D (4%) and E (1%). A subset of 150 records is considered herein to provide a statistically significant number of strong-motion records for seismic fragility curves development using Cloud Analysis approach. The minimum and maximum peak ground acceleration (PGA) of the selected 150 ground motion set are 0.21 and 1.78 g, respectively. In this study, although the chosen ground motion records are not region specific, they are characterized by a reasonably wide range of ground motion features for the generic assessment of the seismic behavior of as-built and deteriorating RC frames.

5.2 | Seismic response comparison of as-built and corroded frames

Before developing seismic fragility curves that explicitly propagate the uncertainty in deteriorating characteristics, a sample deterministic simulation is demonstrated first to elucidate the impact of corrosion deterioration modeling on the

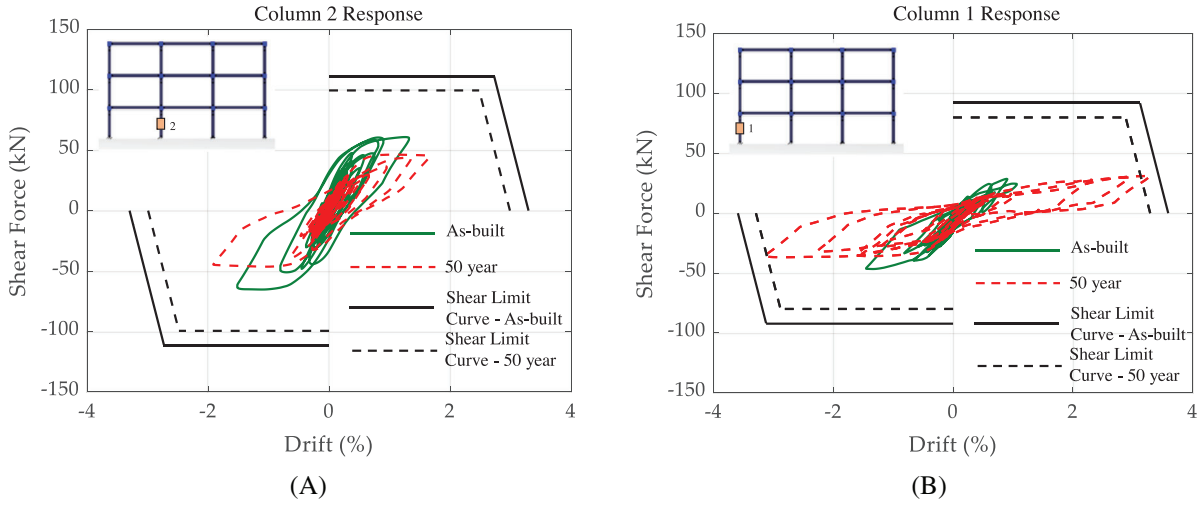

FIGURE 9 Comparison of seismic response of as-built and 50-year corroded frame column for (A) shear force versus drift response of column 2 of ground story and (B) shear force versus drift response of column 1 of ground story.

seismic response and failure modes of the case-study frame. To this end, along with the as-built frame, an aging 50-year corroded frame is considered, where corrosion leads to 19% reduction in steel reinforcement area along with other secondary effects. The FE model of the as-built and 50-year frames with all parameters set to their mean estimates is subjected to two ground motion records from the suite used in this study. Figure 9A shows the comparison of the seismic response of Column 2 (shown in the inset) of the ground story for the as-built and 50-year frame using a low-intensity ground motion record. For this accelerogram, column peak drift increases by about 26% after 50 years of corrosion exposure compared to the as-built column. However, the hysteresis loop of both the as-built and 50-year columns does not intersect the strength or drift limit curve—therefore highlighting no shear failure. On the other hand, for a high-intensity ground motion record, as shown in Figure 9B, the column (Column 1, ground story) peak drift increases by about 127.2% after 50 years of corrosion exposure compared to the as-built column. It is worthwhile to note that the hysteresis loop of the 50-year column intersects the drift-based shear limit curve highlighting the onset of flexure-shear failure. However, the hysteresis loop does not reach either strength or drift shear limit curve for the as-built case, thereby experiencing flexure behavior (Figure 9B). This change in the failure mode of RC column from flexure to flexure-shear due to corrosion is consistent with the past experimental findings as reported earlier in Figure 6.

The results presented in this section correspond to the chosen set of ground motions and deterministic aging frame sample. The implications of these findings on the seismic fragility are further assessed through cloud analysis by considering the selected ground motion suites to capture record-to-record variability. Additionally, uncertainties associated with corrosion deterioration parameters are also considered as the building frame continues to age along its design life.

5.3 | Time-dependent seismic fragility curves

Following the deterministic analysis, the randomness in ground motion record-to-record variability and corrosion deterioration is incorporated within the NLTHAs. For 25- and 50-year corroded frames, 150 statistically different yet nominally identical aging frame models are developed by drawing samples across the range of sample space of corrosion deterioration parameters. The 150 frame models are then randomly paired with 150 records from the selected ground motion set, followed by recording the *EDP* in terms of IDR_{max} after conducting the non-linear time history runs of the FE models. For the development of PSDMs, the selection of an optimal *IM* is critical to reduce the uncertainty in seismic demand prediction. Several past studies on the seismic fragility assessment of building frames[33,75] suggest the use of structure-specific *IM* (such as spectral acceleration at the fundamental time period $[S_a(T_1)]$) as an optimal *IM* for the development of PSDMs and subsequent fragility assessment. However, corrosion deterioration of RC beams and columns leads to a reduced steel rebar area and alterations in mechanical characteristics with a consequent shift of the fundamental structural time period of the building frame. For the case-study structure, Figure 10A shows the elongation in the time period of the frame (due to corrosion) at different points in time along the service life. It should be noted that the corrosion of stirrups has minimal

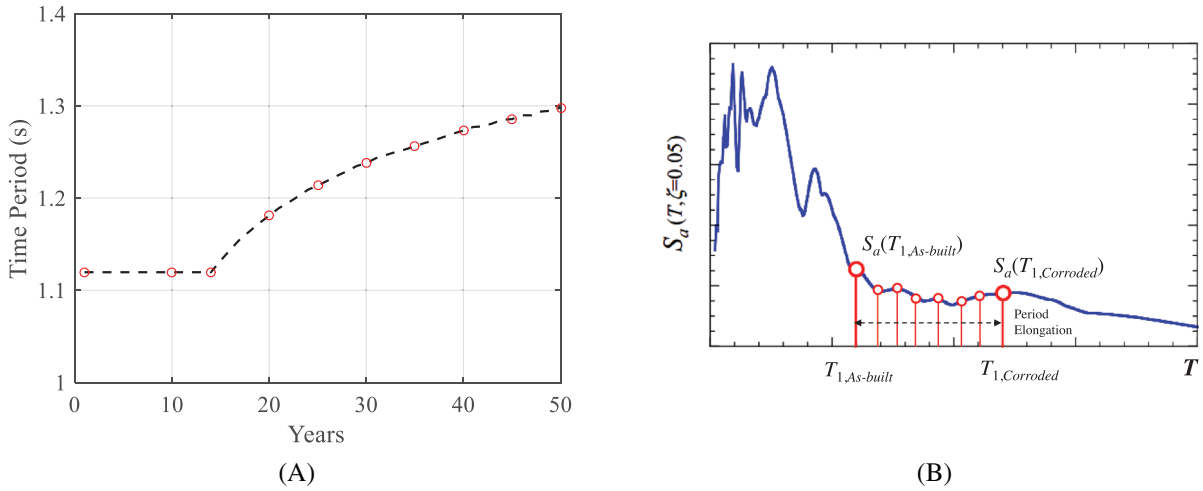

FIGURE 10 (A) Elongation in the time period of the frame (due to corrosion) at different points in time along the service life and (B) schematic representation of chosen *IM*—spectral acceleration of a ground motion record at equally spaced time periods between a lower bound $T_{1,As\text{-}built}$ and an upper bound $T_{1,Corroded}$.

influence on the modulus of elasticity of the concrete, and as a result, it does not affect the structural time period of the frame. However, once corrosion of longitudinal reinforcement begins (14 years), there is an observed increase in the time period. This increase is caused by a decrease in the area of the longitudinal rebar and a reduction in the strength of the cover concrete, which subsequently leads to a decrease in the stiffness of the RC members. The fundamental time period of the as-built and 50-year frames (with corrosion deterioration parameters set at mean values) are estimated as 1.12 and 1.30 s, respectively. Thus, in order to allow the direct comparison of the PSDMs and fragility curves of different frames, the average spectral acceleration is proposed here as *IM* [$S_{a,avg}$ ($T_{1,As\text{-}built}$—$T_{1,Corroded}$,5%)], which is defined as the geometric mean of the discrete spectral acceleration values within the time period ($\Delta T = T_{1,Corroded} - T_{1,As-built}$) as:

$$S_{a,avg}\left(T_{1,As-built} - T_{1,Corroded}, 5\%\right) = \left(\prod_{i=1}^{n} S_a\left(T_{1,n}\right)\right)^{1/n} \tag{3}$$

where, $T_{1,As\text{-}built}$ and $T_{1,Corroded}$ are the fundamental time period of the as-built and corroded frames, n is the number of discrete spectral ordinates between $T_{1,As\text{-}built}$ and $T_{1,Corroded}$. Figure 10B shows the schematic description of the spectral acceleration of a ground motion record at equally spaced time periods between the lower and the upper bounds ($T_{1,As\text{-}built}$ and $T_{1,Corroded}$). The geometric mean of the discrete spectral ordinates is obtained using Equation (3), and is used for the development and comparative assessment of the PSDMs and fragility curves of as-built and corroded frame structures.

For as-built and corroded frames, PSDMs are developed following the power law relationship proposed by Cornell et al.,[31] which in the transformed logarithmic space follows a linear relationship with the ground motion *IM* as:

$$\ln\left[EDP_{med}(t)\right] = \ln r_1(t) + r_2(t)\ln(S_{a,avg}) \tag{4}$$

where, EDP_{med} is the median estimate of *EDP* taken as IDR_{max} in this study, $\ln r_1(t)$ and $r_2(t)$ represent the linear regression coefficients corresponding to a particular instant of time along the service life. The regression relationship also keeps track of the normally distributed zero mean models fitting error (β_D) that aids in the fragility development. Figure 11A shows the comparison of PSDMs of the as-built and 50-year frames. The markers in Figure 11A represent the *IM-EDP* ($S_{a,avg}$—IDR_{max}) pairs obtained from 150 NLTHAs simulations, while the lines represent the linear relationship obtained after regression [Equation (4)]. Note that as depicted earlier in the deterministic analysis, for several high-intensity ground motions, flexure-shear failures are observed in the RC frame columns for both as-built and 50-year frames (Figure 11A). The comparison of the results indicates a higher estimate of the median seismic demand for the 50-year frame as compared with the as-built frame. Also, high R^2 estimates are obtained for both frames, underlining the adequacy of the chosen *IM* [$S_{a,avg}$] for predicting IDR_{max}.

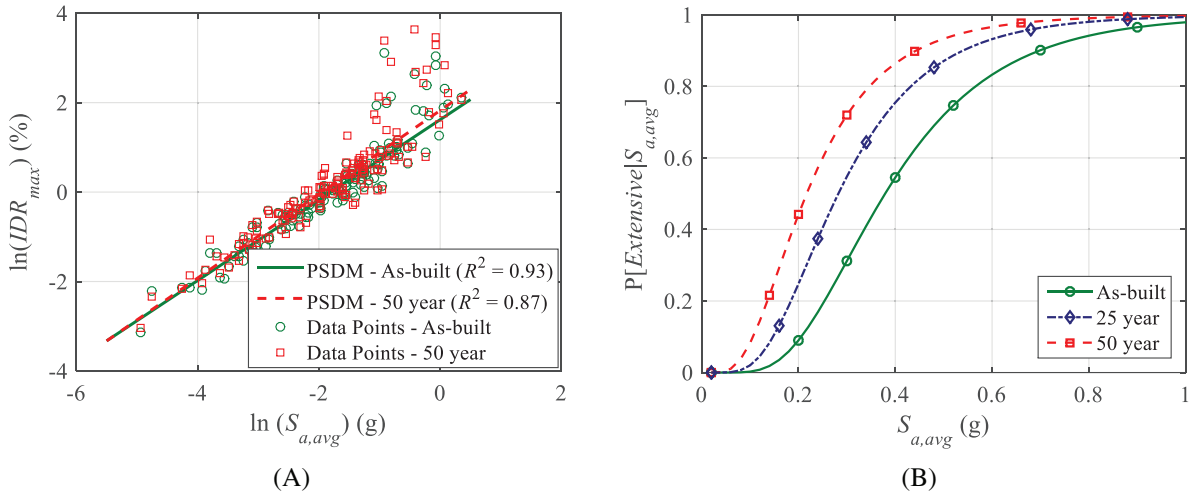

FIGURE 11 (A) Non-linear time history response and fitted PSDMs for as-built and 50-year frames and (B) Extensive *DS* seismic fragility curves for as-built, 25-year, and 50-year frames.

TABLE 3 Median (*med*) and dispersion (ζ) of the seismic fragility curves at different points in time along the design service life.

	Slight		Moderate		Extensive		Complete	
Years	***med***	ζ	***med***	ζ	***med***	ζ	***med***	ζ
As-built	0.109	0.476	0.210	0.476	0.379	0.476	0.554	0.476
25-year	0.097	0.503	0.168	0.504	0.282	0.506	0.398	0.511
50-year	0.076	0.554	0.099	0.600	0.217	0.557	0.339	0.547

The PSDMs and the *DS* thresholds estimates are utilized next to develop seismic fragility curves for the as-built and corroded frames. Assuming that the seismic demand follows lognormal distributions along with *DSs* thresholds, the time-varying seismic fragility curves for a particular *DS* can be expressed as:

$$Pf_{DS|IM}(t) = \Phi\left\{\frac{\ln\left(EDP_{med}\left(t\right)/C_{med}\left(t\right)\right)}{\sqrt{\beta_D^2\left(t\right)+\beta_C^2\left(t\right)}}\right\} = \Phi\left\{\frac{\ln(IM)-\ln(med(t))}{\zeta(t)}\right\} \tag{5}$$

$$med(t) = [\ln[C_{med}(t)] - \ln r_1(t)]/r_2(t) \quad \zeta\left(t\right) = \sqrt{\beta_D^2\left(t\right)+{\beta_C}^2\left(t\right)}/r_2\left(t\right) \tag{6}$$

where, $Pf_{DS|IM}(t)$ represents the seismic fragility of a *DS* at a specific point in time along the service life of the structure, $EDP_{med}(t)$ and $C_{med}(t)$ are the time-dependent *DS* median estimates, respectively, for the seismic demand and *DS* thresholds, $\beta_D(t)$ and $\beta_C(t)$ represent the corresponding lognormal standard deviations of the demand and capacity, while $med(t)$ and $\zeta(t)$ represent the median and dispersion of the lognormal distributed fragility curves. Figure 11B shows the Extensive *DS* seismic fragility curves for the as-built, 25-, and 50-year frames. A significant increase in the vulnerability of 25- and 50-year frames is observed as compared to the as-built frame. The exposure to chlorides deteriorates the RC frame causing a reduction in strength and ductility, resulting in a decrease in *DS* capacities (Figure 8 and Table 2) and an increase in seismic demands (Figure 11A), eventually leading to an increase in vulnerability. Similar increase in fragility due to corrosion is also observed for other *DSs* at different points in time along the service life of the building frame.

Variations in the fragility curves are most easily evaluated by comparing the medians (defined as the median $S_{a,avg}$ corresponding to 50% probability of exceeding a particular *DS*). Table 3 shows the median $S_{a,avg}$ and dispersion of the lognormally distributed fragility curves for the as-built, 25- and 50-year frames. The median $S_{a,avg}$ of 50-year frame are 30%, 53%, 43%, and 38% lower (indicating an increase in vulnerability) than the as-built frame for Slight, Moderate, Extensive, and Complete *DSs*, respectively. For the 25-year frame, these percentage decrease in median $S_{a,avg}$ are 11%, 20%, 26%, and 28%, respectively, for various *DSs*. Furthermore, compared to the as-built frame, 25- and 50-year frames has higher dispersion of fragility curves [$\zeta(t)$]. This is mainly attributed to the increase in demand dispersion [$\beta_D(t)$], capacity dispersion, [$\beta_C(t)$], and slope [$r_2(t)$] resulting from corrosion. In closing, the present section of the paper presents time-dependent

seismic fragility curves of aging low-ductile RC frame accounting for the influence of corrosion deterioration and its associated effects, including period elongation, change in failure modes, time-varying *DSs* thresholds, among others, while also incorporating deterioration uncertainty along with record-to-record variability of ground motion. The results indicate that corrosion deterioration significantly affects the failure modes and seismic fragility of aged non-seismically designed RC frames and must be considered for lifetime seismic fragility assessment of building stocks in seismic-prone regions.

6 | CONDITION-DEPENDENT SEISMIC FRAGILITY FUNCTIONS

Until now, this study has focused on the time-dependent seismic fragility analysis of a low-ductility frame for typical marine exposure conditions by considering the corrosion deterioration model from Duracrete.[42] Numerous assumptions assist these corrosion deterioration models in computing crucial deterioration aspects, such as the initiation time and the rate of corrosion propagation.[2,23] Furthermore, most of these theoretical or empirical corrosion models are based on controlled laboratory experiments, which may differ from in-situ field conditions leading to biased predictions. While this study considers the uncertainty of crucial parameters using probability distributions (Table 1) to evaluate the amount of corrosion deterioration, in-situ field measurements may reveal parameter estimates within or even beyond the tails of assumed distributions leading to significant shifts in the seismic vulnerability.[76] Consequently, time-dependent seismic fragility curves developed in the previous section may become inaccurate representations of the seismic performance of the structure. Therefore, it is desirable to develop more generic condition-dependent fragility functions based on the percentage mass loss of steel as compared to exposure-specific time-dependent fragility functions that are only applicable to chosen exposure scenario and corrosion deterioration model. This section of the paper proposes an approach for computing seismic fragilities for deteriorating frame structures based on the in-situ field observation parameters.

Among the different inputs for seismic fragility analysis of deteriorating frame structure, the time-dependent seismic fragility curves primarily depend on the residual steel reinforcement area along with associated secondary effects such as reduction in concrete and steel mechanical properties. Thus, independent of the exposure scenario, the percentage mass loss of steel (ψ %) may be utilized as a general measure of corrosion to determine the increase in seismic vulnerability of the deteriorating structure. This quantity also serves as a standard measure to determine the degree of corrosion deterioration utilizing widely used destructive or non-destructive (NDT) structural health monitoring techniques, such as x-ray imaging and infra-red thermography, among others.[77–81] Consequently, FE analyses are carried out for the case-study frame for various deterioration levels (0–25% mass loss of steel, ψ %), and based on the results, a simple quadratic polynomial function is derived to estimate the parameters [$med\ (\psi)$, $\zeta(\psi)$] of the fragility curves as a function of percentage mass loss (ψ %). Table 4 shows the quadratic functions of medians and dispersions for all *DSs* that can be used to develop the seismic fragility curves for different deterioration levels independent of the exposure scenario. Note that the percentage mass loss used herein corresponds to area loss of the longitudinal reinforcement in RC frame and also aids in estimating other corrosion deterioration effects, such as reduction in cover concrete strength and steel strength and ductility. The corresponding mass loss for the transverse reinforcement (required for estimating core concrete strength and shear strength degradation) is higher due to a smaller cover depth, and is calculated based on the adopted corrosion deterioration model (Figure 3B). For the case-study frame, Figure 12 shows the application of derived fragility functions and develop a seismic fragility surface conditioned upon the percentage of mass loss and average spectral acceleration as *IM* for Complete *DS*. As the figure shows, when the degree of deterioration is known either from the field measurement or from the standard corrosion deterioration model predictions, the probability of failure given a specific ground motion *IM* can be conveniently computed. Such fragility surfaces can serve as a reference for researchers studying the seismic performance of similar low-ductility RC frames.

TABLE 4 Predictive quadratic functions of fragility parameters as function of percentage of mass loss for various *DSs*.

Damage states	$med\ (\psi)$	$\zeta(\psi)$
Slight	$3.86 \times 10^{-5}\psi^2 - 0.0025\psi + 0.11$	$-6.55 \times 10^{-5}\psi^2 + 0.0038\psi + 0.48$
Moderate	$1.11 \times 10^{-4}\psi^2 - 0.0083\psi + 0.28$	
Extensive	$4.02 \times 10^{-4}\psi^2 - 0.0172\psi + 0.39$	
Complete	$7.09 \times 10^{-4}\psi^2 - 0.0266\psi + 0.57$	

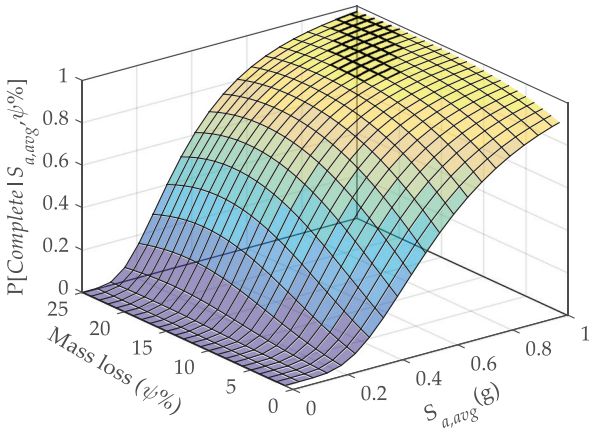

FIGURE 12 Seismic fragility surface of low-ductile RC frame for Complete damage state considering different percentages of mass loss of longitudinal rebar.

7 | CONCLUSIONS

This study proposes a probabilistic framework to assess and quantify the influence of corrosion deterioration on the failure mechanisms and seismic vulnerability of low-ductility RC frames. Corrosion deterioration of RC members results in a significant reduction of frame lateral load-carrying capacity and may lead to non-ductile shear failure. This study utilizes an experimentally validated numerical model that can capture varying failure in aging low-ductility RC frames under seismic loads and develops seismic fragility curves incorporating uncertainty of corrosion deterioration parameters and ground motion record-to-record variability. The following are some of the important conclusions that can be drawn from the present study:

- Corrosion of RC frame primarily leads to loss of cross-sectional area and other secondary effects such as reduction of concrete and steel strength, and loss of ductility. For the considered exposure scenario, at the end of 50 years of service life, probabilistic modeling of chloride-induced corrosion reveals 19% and 38% mean reduction in rebar area loss for longitudinal and transverse reinforcement, respectively. Additionally, corrosion also leads to several secondary effects, and at the end of 50 years, RC columns experience 79%, 10%, 67%, and 25% mean reduction in the cover concrete strength, steel strength, ultimate steel strain, and shear strength, respectively.
- Corrosion of RC columns significantly impairs the lateral load capacity of the RC frames. Non-linear static analyses reveal a 25% reduction in the mean lateral load capacity of the 50-year corroded frame as compared to the as-built frame. Additionally, the median damage state threshold (obtained after mapping from local to global *EDP*, that is, maximum inter-story drift ratio) of 50-year corroded RC frame for Slight, Moderate, Extensive, and Complete damage states are 19%, 43%, 30%, and 24% lower when compared to those for the as-built frame.
- Deterministic seismic response results reveal a change in the failure mechanism of some frame components from flexure to flexure-shear as a consequence of corrosion. The column peak drifts also increase significantly (by about 127%) after 50 years of corrosion exposure compared to the as-built frame. Additionally, as corrosion deterioration elongates the fundamental time period of the frame, this study suggests the use of average spectral acceleration considering the period range of the as-built and corroded frames [$S_{a,avg}$ ($T_{1,As\text{-}built}$−$T_{1,Corroded}$,5%)] as *IM* allowing the comparison of the respective fragility curves.
- The combined effect of corrosion deterioration and earthquake significantly influences the failure probability of the RC frame. The percentage decrease in median $S_{a,avg}$ (indicating increase in vulnerability) of Extensive *DS* are 28% and 38%, respectively, for 25-year and 50-year old corroded RC frames.
- In addition to comparative seismic fragility assessment for chosen standard exposure conditions, this study proposes condition-dependent seismic fragility functions conditioned upon the degree of corrosion deterioration and ground motion *IM* ($S_{a,avg}$). Such functions aid in the prompt assessment of seismic fragility of similar low-ductility RC frames for varied exposure scenarios.

The obtained results underline the necessity of considering the influence of aging and deterioration on the lifetime seismic vulnerability of older building stocks in seismic-prone regions. While the results presented herein are specific to the case-study structure under the specified exposure condition, the proposed framework can be extended to other building typologies to assess the impact of corrosion deterioration on aged building seismic fragility. Future studies should investigate the influence of non-uniform distribution of corrosion within the structural elements and spatial correlation of corrosion between the building elements on the seismic fragility of RC buildings.

ACKNOWLEDGMENTS

The first author would like to acknowledge the funding from Science and Engineering Research Board (statutory body under the Department of Science and Technology, India) through Grant No. SRG/2021/001574 for this work. The third author gratefully acknowledges the funding provided by the Science and Engineering Research Board (statutory body under the Department of Science and Technology, India) through Grant No. CRG/2021/000777. Any opinions, findings, conclusions, or recommendations expressed in this paper are those of the authors and do not necessarily reflect the views of the funding agencies.

DATA AVAILABILITY STATEMENT

The data that support the findings of this study are available from the corresponding author upon reasonable request.

ORCID

Shivang Shekhar https://orcid.org/0000-0003-0474-4202
Fabio Freddi https://orcid.org/0000-0003-2048-1166
Jayadipta Ghosh https://orcid.org/0000-0002-5655-9730

REFERENCES

1. Qing Li C. Reliability based service life prediction of corrosion affected concrete structures. *J Struct Eng*. 2004;130(10):1570-1577.
2. Broomfield JP. *Corrosion of Steel in Concrete: Understanding, Investigation and Repair, Second Edition*. CRC Press; 2006.
3. Angst UM. Challenges and opportunities in corrosion of steel in concrete. *Mater Struct*. 2018;51:1-20.
4. Koch G, Varney J, Thompson N, Moghissi O, Gould M, Payer J. International measures of prevention, application, and economics of corrosion technologies study. *NACE Int*. 2016;216:2-3.
5. Davis C, Keilis-Borok V, Kossobokov V, Soloviev A. Advance prediction of the March 11, 2011 Great East Japan Earthquake: a missed opportunity for disaster preparedness. *Int J Disaster Risk Reduct*. 2012;1:17-32.
6. Wu J, Li N, Xie W, Zhou Y, Ji Z, Shi P. Post-disaster recovery and economic impact of catastrophes in China. *Earthq Spectra*. 2014;30(4):1825-1846.
7. Ghosh J, Padgett JE. Aging considerations in the development of time-dependent seismic fragility curves. *J Struct Eng*. 2010;136(12):1497-1511.
8. Choe DE, Gardoni P, Rosowsky D, Haukaas T. Seismic fragility estimates for reinforced concrete bridges subject to corrosion. *Struct Saf*. 2009;31(4):275-283.
9. Alipour A, Shafei B, Shinozuka M. Performance evaluation of deteriorating highway bridges located in high seismic areas. *J Bridge Eng*. 2011;16(5):597-611.
10. Pitilakis KD, Karapetrou ST, Fotopoulou SD. Consideration of aging and SSI effects on seismic vulnerability assessment of RC buildings. *Bull Earthq Eng*. 2014;12(4):1755-1776.
11. Couto R, Requena-García-Cruz MV, Bento R, Morales-Esteban A. Seismic capacity and vulnerability assessment considering ageing effects:case study—three local Portuguese RC buildings. *Bull Earthq Eng*. 2020;19:6591-6614.
12. Di Sarno L, Pugliese F. Numerical evaluation of the seismic performance of existing reinforced concrete buildings with corroded smooth rebars. *Bull Earthq Eng*. 2020;18(9):4227-4273.
13. Dizaj EA, Madandoust R, Kashani MM. Probabilistic seismic vulnerability analysis of corroded reinforced concrete frames including spatial variability of pitting corrosion. *Soil Dyn Earthq Eng*. 2018;114:97-112.
14. Di Sarno L, Pugliese F. Seismic fragility of existing RC buildings with corroded bars under earthquake sequences. *Soil Dyn Earthq Eng*. 2020;134:106169.
15. Freddi F, Ghosh J, Kotoky N, Raghunandan M. Device uncertainty propagation in low-ductility RC frames retrofitted with BRBs for seismic risk mitigation. *Earthq Eng Struct Dyn*. 2021;50(9):2488-2509.
16. Meda A, Mostosi S, Rinaldi Z, Riva P. Experimental evaluation of the corrosion influence on the cyclic behaviour of RC columns. *Eng Struct*. 2014;76:112-123.
17. Goksu C, Ilki A. Seismic behavior of reinforced concrete columns with corroded deformed reinforcing bars. *ACI Struct J*. 2016;113(5):1053-1064.
18. Ma Y, Che Y, Gong J. Behavior of corrosion damaged circular reinforced concrete columns under cyclic loading. *Constr Build Mater*. 2012;29:548-556.

19. Yang SY, Song XB, Jia HX, Chen X, Liu XL. Experimental research on hysteretic behaviors of corroded reinforced concrete columns with different maximum amounts of corrosion of rebar. *Constr Build Mater*. 2016;121:319-327.
20. Rinaldi Z, Di Carlo F, Spagnuolo S, Meda A. Influence of localised corrosion on the cyclic response of reinforced concrete columns. *Eng Struct*. 2022;256:114037.
21. Vu NS, Li B. Seismic performance of flexural reinforced concrete columns with corroded reinforcement. *ACI Struct J*. 2018;115(5):1253-1266.
22. Li Q, Niu DT, Xiao QH, Guan X, Chen SJ. Experimental study on seismic behaviors of concrete columns confined by corroded stirrups and lateral strength prediction. *Constr Build Mater*. 2018;162:704-713.
23. Bertolini L, Elsener B, Pedeferri P, Polder RB. *Corrosion of Steel in Concrete: Prevention, Diagnosis, Repair*. Wiley-VCH; 2004.
24. Freddi F, Tubaldi E, Ragni L, Dall'Asta A. Probabilistic performance assessment of low-ductility reinforced concrete frames retrofitted with dissipative braces. *Earthq Eng Struct Dyn*. 2013;42(7):993-1011.
25. Freddi F, Padgett JE, Dall'Asta A. Probabilistic seismic demand modeling of local level response parameters of an RC frame. *Bull Earthq Eng*. 2017;15(1):1-23.
26. Gutierrez-Urzua F, Freddi F, Di Sarno L. Comparative analysis of code-based approaches for seismic assessment of existing steel moment resisting frames. *J Constr Steel Res*. 2021;181:106589.
27. Gutiérrez-Urzúa LF, Freddi F. Influence of the design objectives on the seismic performance of steel moment resisting frames retrofitted with buckling restrained braces. *Earthq Eng Struct Dyn*. 2022;51(13):3131-3153.
28. Opabola E. Residual seismic capacity of beam-column components with corroded reinforcement. *Constr Build Mater*. 2022;332:127269.
29. FEMA. *Multi-Hazard Loss Estimation Methodology Earthquake Model. FEMA HAZUS-MH MR 1*, Federal Emergency Management Agency; 2002.
30. Aljawhari K, Gentile R, Freddi F, Galasso C. Effects of ground-motion sequences on fragility and vulnerability of case-study reinforced concrete frames. *Bull Earthq Eng*. 2021;19:6329-6359.
31. Cornell C, Jalayer F, Hamburger RO, Foutch DA. Probabilistic basis for 2000 SAC federal emergency management agency steel moment frame guidelines. *J Struct Eng*. 2002;128(4):526-533.
32. Belletti B, Vecchi F. A crack model for corroded reinforced concrete elements subject to cyclic loading. *Proc Inst Civil Eng Bridge Eng*. 2022;175(1):50-65.
33. Jeon JS, Lowes LN, DesRoches R, Brilakis I. Fragility curves for non-ductile reinforced concrete frames that exhibit different component response mechanisms. *Eng Struct*. 2015;85:127-143.
34. Bracci JM, Reinhorn AM, Mander JB. Seismic resistance of reinforced concrete frame structures designed for gravity loads:performance of structural system. *ACI Struct J*. 1995;92(5):597-609.
35. 318 AC. *Building Code Requirements for Reinforced Concrete and Commentary (ACI 318–89/ACI 318R-89)*. American Concrete Institute; 1989.
36. Aycardi L, Mander J, Reinhorn A. Seismic resistance of reinforced concrete frame structures designed only for gravity loads: experimental performance of subassemblages. *ACI Struct J*. 1994;91(5):552-563.
37. Stewart MG, Rosowsky DV. Time-dependent reliability of deteriorating reinforced concrete bridge decks. *Struct Saf*. 1998;20(1):91-109.
38. Akiyama M, Frangopol DM, Matsuzaki H. Life-cycle reliability of RC bridge piers under seismic and airborne chloride hazards. *Earthq Eng Struct Dyn*. 2011;40(15):1671-1687.
39. Zhang Y, Ayyub BM, Fung JF. Projections of corrosion and deterioration of infrastructure in United States coasts under a changing climate. *RCS*. 2022;1(1):98-109.
40. Thoft-Christensen P. Modelling of Corrosion Cracks. Information Processing: Recent Mathematical Advances in Optimization and Control: Articles from the IFIP TC 7 Conference on System Modelling and Optimization, Sophia Antipolis, France; 2004.
41. Bojorquez J, Ponce S, Ruiz SE, et al. Structural reliability of reinforced concrete buildings under earthquakes and corrosion effects. *Eng Struct*. 2021;237:112161.
42. Duracrete. Probabilistic performance based durability design of concrete structures: final technical report. The European Union—Brite EuRam III. 2000.
43. Ou YC, Fan HD, Nguyen ND. Long-term seismic performance of reinforced concrete bridges under steel reinforcement corrosion due to chloride attack. *Earthq Eng Struct Dyn*. 2013;42(14):2113-2127.
44. Vu KAT, Stewart MG. Structural reliability of concrete bridges including improved chloride-induced corrosion models. *Struct Saf*. 2000;22(4):313-333.
45. Ahmad S, Bhattacharjee B. Empirical modeling of indicators of chloride-induced rebar corrosion. *J Struct Eng*. 2000;27(3):195-207.
46. Stewart MG. Spatial variability of pitting corrosion and its influence on structural fragility and reliability of RC beams in flexure. *Struct Saf*. 2004;26(4):453-470.
47. Coronelli D, Gambarova P. Structural assessment of corroded reinforced concrete beams: modeling guidelines. *J Struct Eng*. 2004;130(8):1214-1224.
48. Mander JB, Priestley M, Park R. Theoretical stress-strain model for confined concrete. *J Struct Eng*. 1988;114(8):1804-1826.
49. Du YG, Clark LA, Chan AHC. Residual capacity of corroded reinforcing bars. *Mag Concr Res*. 2005;57(3):135-147.
50. Andisheh K, Scott A, Palermo A. Seismic behavior of corroded RC bridges: review and research gaps. *Int J Corros*. 2016:1-22.
51. Apostolopoulos CA, Papadakis VG. Consequences of steel corrosion on the ductility properties of reinforcement bar. *Constr Build Mater*. 2008;22(12):2316-2324.
52. Chen E, Berrocal CG, Fernandez I, Löfgren I, Lundgren K. Assessment of the mechanical behaviour of reinforcement bars with localised pitting corrosion by digital image correlation. *Eng Struct*. 2020;219:110936.

53. Kashani MM, Alagheband P, Khan R, Davis S. Impact of corrosion on low-cycle fatigue degradation of reinforcing bars with the effect of inelastic buckling. *Int J Fatigue*. 2015;77:174-185.
54. Rao AS, Lepech MD, Kiremidjian AS, Sun XY. Simplified structural deterioration model for reinforced concrete bridge piers under cyclic loading. *Struct Infrastruct Eng*. 2017;13(1):55-66.
55. Fang C, Lundgren K, Plos M, Gylltoft K. Bond behaviour of corroded reinforcing steel bars in concrete. *Cem Concr Res*. 2006;36(10):1931-1938.
56. Wang X, Liu X. Modeling bond strength of corroded reinforcement without stirrups. *Cem Concr Res*. 2004;34(8):1331-1339.
57. Cui F, Zhang H, Ghosn M, Xu Y. Seismic fragility analysis of deteriorating RC bridge substructures subject to marine chloride-induced corrosion. *Eng Struct*. 2018;155:61-72.
58. Kowalsky MJ. Deformation limit states for circular reinforced concrete bridge columns. *J Struct Eng*. 2000;126(8):869-878.
59. Kashani MM, Lowes LN, Crewe AJ, Alexander NA. Phenomenological hysteretic model for corroded reinforcing bars including inelastic buckling and low-cycle fatigue degradation. *Comput Struct*. 2015;156:58-71.
60. Pelle A, Briseghella B, Bergami AV, et al. Time-dependent cyclic behavior of reinforced concrete bridge columns under chlorides-induced corrosion and rebars buckling. *Struct Concr*. 2022;23(1):81-103.
61. McKenna F, Fenves GL, Scott MH. Open System for Earthquake Engineering Simulation. Berkeley, CA: University of California; 2006.
62. Panagiotakos TB, Fardis MN. Deformation of reinforced concrete at yielding and untimate. *ACI Struct J*. 2001;98(2):135-147.
63. Elwood KJ. Modelling failures in existing reinforced concrete columns. *Can J Civ Eng*. 2004;31(5):846-859.
64. Shekhar S, Ghosh J, Ghosh S. Impact of design code evolution on the failure mechanism and seismic fragility of highway bridge piers. *J Bridge Eng ASCE*. 2020;25(2):04019140.
65. Baradaran-Shoraka M, Elwood KJ. Mechanical model for non-ductile reinforced concrete columns. *J Earthq Eng*. 2013;17(7):937-957.
66. Zhang X, Li B. Seismic performance of exterior reinforced concrete beam-column joint with corroded reinforcement. *Eng Struct*. 2021;111556:111556.
67. Sezen H. *Seismic Behavior and Modeling of Reinforced Concrete Building Columns*. University of California; 2002.
68. Ghee A, Priestley M, Paulay T. Seismic shear strength of circular reinforced concrete columns. *ACI Struct J*. 1989;86(1):45-59.
69. Rossetto T, Gehl P, Minas S, et al. FRACAS: a capacity spectrum approach for seismic fragility assessment including record-to-record variability. *Eng Struct*. 2016;125:337-348.
70. Ni Choine M. *Seismic reliability assessment of aging integral bridges*. Ph.D. Thesis, Trinity College Dublin. 2014.
71. Ghosh J, Sood P. Consideration of tme-tvolving capacity distributions and improved degradation models for seismic fragility assessment of aging highway bridges. *Reliab Eng Syst Saf*. 2016;154:197-218.
72. Titi A, Bianchi S, Biondini F, Frangopol DM. Influence of the exposure scenario and spatial correlation on the probabilistic life-cycle seismic performance of deteriorating RC frames. *Struct Infrastruct Eng*. 2018;14(7):986-996.
73. Ramanathan KN. *Next Generation Seismic Fragility Curves for California Bridges Incorporating the Evolution in Seismic Design Philosophy*. Georgia Institute of Technology; 2012.
74. Smerzini C, Galasso C, Iervolino I, Paolucci R. Ground motion record selection based on broadband spectral compatibility. *Earthq Spectra*. 2014;30(4):1427-1448.
75. Afsar Dizaj E, Salami MR, Kashani MM. Seismic vulnerability assessment of ageing reinforced concrete structures under real mainshock-aftershock ground motions. *Struct Infrastruct Eng*. 2022;18(12):1674-1690.
76. Shekhar S, Ghosh J, Padgett JE. Seismic life-cycle cost analysis of ageing highway bridges under chloride exposure conditions:modelling and recommendations. *Struct Infrastruct Eng*. 2018;14(7):941-966.
77. Michel A, Pease B, Geiker M, Stang H. *Monitoring Reinforcement Corrosion and Corrosion-Induced Cracking using Non-Destructive X-Ray Attenuation Measurements*. Cement and Concrete; 2011.
78. Akiyama M, Frangopol DM, Estimation of steel weight loss due to corrosion in RC members based on digital image processing of x-ray photogram. Life-Cycle and Sustainability of Civil Infrastructure Systems:Proceedings of the Third International Symposium on Life-Cycle Civil Engineering (IALCCE'12), Vienna, Austria: CRC Press; 2012.
79. Thanapol Y, Akiyama M, Frangopol DM. Updating the seismic reliability of existing RC structures in a marine environment by incorporating the spatial steel corrosion distribution: application to bridge piers. *J Bridge Eng*. 2016;21(7):1-17.
80. Lim S, Akiyama M, Frangopol DM. Assessment of the structural performance of corrosion-affected RC members based on experimental study and probabilistic modeling. *Eng Struct*. 2016;127:189-205.
81. Lim S, Akiyama M, Frangopol DM, Jiang H. Experimental investigation of the spatial variability of the steel weight loss and corrosion cracking of reinforced concrete members: novel x-ray and digital image processing techniques. *Struct Infrastruct Eng*. 2017;13(1):118-134.

How to cite this article: Shekhar S, Freddi F, Ghosh J, Lad D. Influence of corrosion on failure modes and lifetime seismic vulnerability assessment of low-ductility RC frames. *Earthquake Engng Struct Dyn*. 2023;1-23. https://doi.org/10.1002/eqe.4004

APPENDIX

TABLE A1 Summary of experimental column dataset used for numerical model validation.

Properties	Specimen 1[67]	Specimen 19[68]	Specimen U2[21]	Specimen C5[21]
Geometry	Square (457.2 mm sides)	Circular (400 mm diameter)	Square (350 mm sides)	Square (350 mm sides)
Experiment test configuration	Double curvature	Single curvature (cantilever)	Double curvature	Double curvature
Failure type	Flexure-shear	Shear	Flexure	Flexure-shear
Material properties	f_c = 21.1 MPa; f_{yl} = 434.4 MPa; f_{yt} = 476 MPa	f_c = 34.4 MPa; f_{yl} = 436 MPa; f_{yt} = 326 MPa	f_c = 38.1 MPa; f_{yl} = 550 MPa; f_{yt} = 300 MPa	f_c = 38.1 MPa; f_{yl} = 550 MPa; f_{yt} = 300 MPa
Longitudinal and transverse reinforcement	8–28.7 mm bars, 9.5 mm at 304.8 mm spacing	20–16 mm bars, 6 mm at 80 mm spacing	8–20 mm bars, 7.8 mm at 50 mm spacing	8–20 mm bars, 7.8 mm at 50 mm spacing
Axial load ratio	0.151	0.10	0.25	0.25
Aspect ratio	3.22	1.5	2.54	2.54
Corrosion level (%)	–	–	–	3.9% long. rebars, 15.5% stirrups